Received 17 October 2018; revised 22 November 2018; accepted 28 November 2018. Date of publication 30 November 2019;
date of current version 1 March 2019. The review of this paper was arranged by Editor C. Surya.

Digital Object Identifier 10.1109/JEDS.2018.2884253

Comprehensive Analysis and Optimal Design of Ge/GeSn/Ge p-n-p Infrared Heterojunction Phototransistors

ANKIT KUMAR PANDEY [1] (Student Member, IEEE), RIKMANTRA BASU [1] (Member, IEEE), HARSHVARDHAN KUMAR [1], AND GUO-EN CHANG [2,3] (Member, IEEE)

1 Department of Electronics and Communication Engineering, National Institute of Technology Delhi, New Delhi 110040, India
2 Department of Mechanical Engineering, National Chung Cheng University, Chiayi 62102, Taiwan
3 Advanced Institute of Manufacturing With High-Tech Innovations, National Chung Cheng University, Chiayi 62102, Taiwan

CORRESPONDING AUTHORS: R. BASU AND G.-E. CHANG (e-mail: rikmantrabasu@nitdelhi.ac.in; imegec@ccu.edu.tw)

This work was supported in part by the Ministry of Science and Technology of Taiwan under Project MOST 104-2923-E-194-003-MY3 and Project MOST 106-2628-E-194-003-MY2, in part by the Advanced Institute of Manufacturing with High-Tech Innovations through the Featured Areas Research Center Program within the Framework of the Higher Education Sprout Project by the Ministry of Education in Taiwan, and in part by the India–Taiwan Program in Science and Technology under Project GITA/DST/TWN/P-63/2015. The work of H. Kumar was supported by DST-SERB, Govt. of India, through Early Career Research Award Scheme 2017 under Grant ECR/2017/000794.

ABSTRACT We present a comprehensive analysis of practical p-n-p Ge/$Ge_{1-x}Sn_x$/Ge heterojunction phototransistors (HPTs) for design optimization for efficient infrared detection. Our design includes a $Ge_{1-x}Sn_x$ narrow-bandgap semiconductor as the active layer in the base layer, enabling extension of the photodetection range from near-infrared to mid-infrared to perform wide-range infrared detection. We calculate the current gain, signal-to-noise ratio (SNR), and optical responsivity and investigate their dependences on the structural parameters to optimize the proposed $Ge_{1-x}Sn_x$ p-n-p HPTs. The results show that the SNR is strongly dependent on the operation frequency and that the introduction of Sn into the base layer can improve the SNR in the high-frequency region. In addition, the current gain strongly depends on the Sn content in the $Ge_{1-x}Sn_x$ base layer, and a Sn content of 6%–9% maximizes the optical responsivity achievable in the infrared range. These results provide useful guidelines for designing and optimizing practical p-n-p $Ge_{1-x}Sn_x$ HPTs for high-performance infrared photodetection.

INDEX TERMS GeSn alloys, current gain, sign-to-noise ratio, heterojunction phototransistors, infrared.

I. INTRODUCTION

Heterojunction phototransistors (HPTs) are suitable alternatives to conventional photodetectors (PDs) in infrared photonics applications such as optical communication and light detection and ranging devices owing to their high responsivities, high gains, and high signal-to-noise ratios (SNRs) [1], [2]. For years, *p-i-n* PDs and avalanche photodiodes (APDs) have been utilized at the present telecommunication wavelengths. However, despite having high quantum efficiencies, *p-i-n* PDs possess no internal gain, which limits their sensing performance. Although internal gain is present in APDs, they suffer from high internal noise due to the avalanche multiplication process [3]. Another disadvantage of using APDs is their high operating voltage [4]. All of these problems can be alleviated by using high-performance HPTs in infrared photonic systems [1], [5]–[8].

Silicon (Si) and germanium (Ge) have emerged as the preferred group IV elements for photonic and electronic integration [9] in addition to the well-recognized electronic and energy applications [10]–[14]. Higher reliability and lower cost are expected to be achievable by monolithically integrating group IV materials rather than group III-V materials on Si. However, the realization of efficient photonic devices is challenging because of the indirect bandgap nature of Ge and Si. In addition, their relatively large bandgaps make it difficult to achieve effective optical detection at the telecommunication C-band and beyond, thus making them less useful in telecommunication applications. In this regard,

germanium–tin (GeSn) alloy has emerged as a potential candidate for applications in various optoelectronic devices [15]. The compatibility of GeSn alloy with current complementary metal–oxide-semiconductor (CMOS) technology, its direct bandgap nature, and its high absorption coefficient make it an attractive candidate for use in high-performance PDs [16]–[22]. More than 10 times the absorption coefficient in the C-band and 20 times that in the L-band compared to those of pure Ge can be achieved by proper selection of the Sn composition in $Ge_{1-x}Sn_x$ alloy [23]. In addition, the low-temperature growth of $Ge_{1-x}Sn_x$ on Si provides a pathway for GeSn-based group IV photonics [21]. $Ge_{1-x}Sn_x$ with up to 25% Sn composition has been grown on a Si substrate using molecular beam epitaxy [24]. Various GeSn-based *p-i-n* PDs have also been reported in [16]–[22]. The applications of GeSn alloys in *n-p-n* HPTs (which have the advantage of low-voltage operation) for communication and in the mid-infrared region have been theoretically demonstrated in recent studies [25]–[28]. Recently, a floating-base *n-p-n* GeSn HPT was fabricated with 6.5% Sn composition having a GeSn base for operation at 1550 nm and 2003 nm [29] with a responsivity 10 times greater than those of conventional GeSn-based *p-i-n* PDs, showing great promise as an alternative to conventional PDs for high-performance photodetection. In addition, variation of the Sn content in GeSn alloy causes the detection range to shift because the bandgap energy changes with variation in the Sn content. Therefore, GeSn-based HPTs could be the perfect replacement for conventional PDs to achieve desirable responsivity and a wide detection range from fiber-optic telecommunication wavelengths to the mid- infrared region. However, the performance of HPTs is strongly dependent on their structural parameters. For example, recombination in the base region can be reduced by using a low base thickness, which enhances the current gain. However, punch-through may occur if the base region is too thin. Reasonable emitter injection efficiency can be maintained by having a low-doped base region, and proper selection of the base region thickness can result in a base transport factor of unity [30], [31]. However, the base resistance will become high with low base doping, limiting the high-frequency operation of the device [31]. Thus, optimization of the layer thickness and doping is important in enhancing device performance [32]. Furthermore, although *n-p-n* GeSn HPTs have been proposed and studied, a heavily *n*-type doping concentration $> 10^{19}$ cm^{-3} in the Ge emitter layer is usually favorable in achieving a high current gain [25], [28]. However, from the viewpoint of epitaxy, the limited donor solubility makes it challenging to achieve such a high *n*-doping level in Ge while maintaining good material quality [33]. Meanwhile, *p-n-p* GeSn HPTs may have the potential to achieve high current gain and quantum efficiency because of the availability of heavily *p*-type doping of $> 10^{20}$ cm^{-3} in Ge, which could enable this issue to be overcome [34]. In addition, Shao *et al.* [30], who investigated an AlGaAsSb–InGaAsSb heterojunction, predicted that *p-n-p* HPTs could provide higher emitter injection ratios than *n-p-n* HPTs, leading to higher quantum efficiencies. Therefore, it is very interesting to study the performance of *p-n-p* GeSn HPTs for use in infrared photonic applications.

In this research, a practical three-terminal *p-n-p* GeSn HPT with a common emitter configuration was developed and theoretically studied. We calculate the terminal currents, DC current gain, SNR, reflectivity, and optical responsivity of the proposed GeSn HPT. We then investigate the effects of the Sn composition in the base layer and the structural parameters on the performance to optimize the structure for maximal optical responsivity.

The remainder of this paper is organized as follows. Section I provides an introduction of the HPT device structure and the layer parameters used in the simulation process in Section II. The theoretical models are presented in Section III. The results and discussion are presented in Section IV, and the conclusions are drawn in Section V.

II. DEVICE STRUCTURE

Figure 1(a) shows our proposed normal-incident three-terminal $Ge_{1-x}Sn_x$ *p-n-p* HPT on a Si (001) substrate, which consists of a four-layered structure (starting from the substrate): (a) a fully strain-relaxed Ge virtual substrate (VS), (b) a *p*-type Ge collector, (c) an *n*-type GeSn base layer, and (d) a *p*-type Ge emitter. The device parameters, including the doping concentrations, thicknesses, and conductivity types, are summarized in Table 1. Considering that the $Ge_{1-x}Sn_x$ base was thin, with less than the critical thickness of 200 nm for $x = 10\%$, pseudomorphic stacking was assumed for the HPT structure on the Ge VS [35]; therefore, there was a strain (ε) of $-0.143x$ in the $Ge_{1-x}Sn_x$ base, whereas the Ge layers were strain-free. $Ge_{1-x}Sn_x$ was chosen as the base material for the device because its band gap is smaller than that of Ge, yielding a wider absorption range in the infrared region and larger absorption coefficient than Ge. A SiO_2 layer was employed as an antireflection (AR) layer to minimize the reflected light and to serve as an electrical isolator. Fig. 1(b) shows a schematic band diagram of the proposed *p-n-p* GeSn HPT. Under optical illumination, electrons and holes are generated at the base. These holes are swept towards the *p*-type Ge collector by the built-in electric field. The electrons are accumulated in the base region, as the emitter region has a larger band gap than the base. The base–emitter barrier is reduced by the accumulation of electrons in the base region, allowing the injection of free holes from the emitter into the base region, which diffuse towards the collector region. The initial photocurrent is amplified by this diffusion, eventually leading to optical responsivity enhancement.

III. THEORETICAL MODELS

We adopted the model-solid theory and deformation potential theory to calculate the energy levels and line up the various bands for the strained GeSn HPTs [25], [36]. The band structures were then calculated using the multi-band $\mathbf{k}\cdot\mathbf{p}$ method.

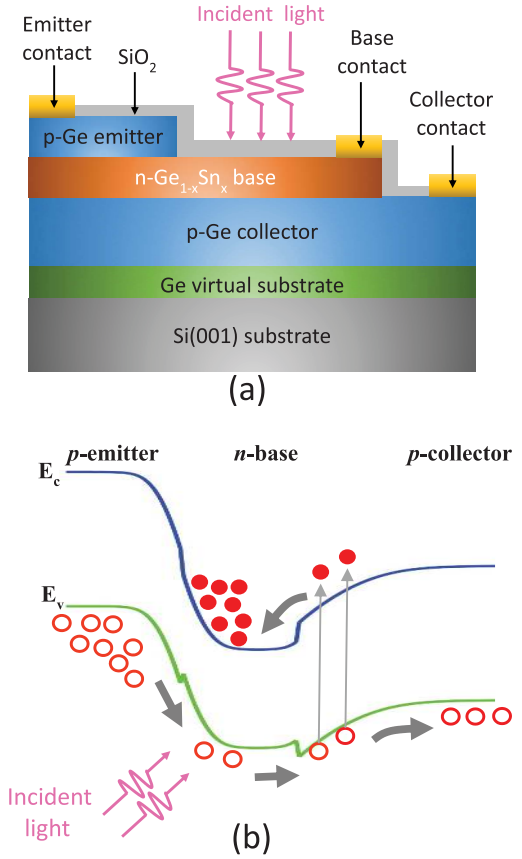

FIGURE 1. (a)Schematic diagram and (b) band diagram of the proposed normal-incident *p-n-p* $Ge_{1-x}Sn_x$ HPT.

TABLE 1. Materials and layered structure of the GeSn heterojunction phototransistor (HPT).

Layer	Material	Thickness t (nm)	Doping level (cm^{-3})	Type
Emitter	Ge	100	2×10^{18}	p
Base	$Ge_{1-x}Sn_x$	50	8×10^{18}	n
Collector	Ge	400	2×10^{17}	p
Virtual substrate	Ge	120	–	i
Substrate	Si	-	–	i

The other theoretical models used in the calculations, including those for the direct-gap interband optical absorption coefficient, DC current gain, and optical responsivity are available in [25] and [28]. To calculate the current gain, a low optical illumination (P_{in}) of 1 μW was assumed, making the generated photocurrent usually linearly proportional to the incident optical power. Therefore, the DC current gain is independent of the incident optical power. Another unique advantage of HPTs is their excellent SNRs compared with those of APDs. The SNR of an HPT is defined as the ratio of the output signal power to the mean square output noise power and depends on the transfer function ($H(f)$) of the small signal equivalent circuit under illumination, which is given by [37]

$$H(f) = \frac{g_{mop}}{g_{\pi op} + j2\pi f[C_{\pi op} + C_{\mu op}(1 - A_V)]}, \tag{1}$$

where f is the operating frequency, g_{mop} is the transconductance under illumination, $g_{\pi op}$ is the equivalent input conductance under illumination, $C_{\pi op}$ is the capacitance under illumination, and $C_{\mu op}$ is the parasitic capacitance. In addition, A_V is the voltage gain of the circuit, which is given by

$$A_V = \frac{-g_{mop} + j2\pi f C_{\mu op}}{\frac{1}{R_i} + j2\pi f C_{\mu op}}, \tag{2}$$

where R_i is the input resistance. The output signal power is defined as

$$S = I_p h^2 |H(f)|^2 R_{eq}, \tag{3}$$

where R_{eq} is the equivalent output resistance and I_{ph} is the photo-generated current. The output noise power is given by [32]

$$N = \bar{i}_n^2(t) R_{eq}, \tag{4}$$

where $\bar{i}_n^2$ is the mean square output noise current, which accounts for the shot noise power at the base–emitter and base–collector junctions as well as the thermal noise power [37]. By using equations (3) and (4), the SNR of the HPT can be calculated using

$$SNR = \frac{I_{ph}^2 |H(f)|^2}{\bar{i}_n^2(t)}. \tag{5}$$

Taking the parameters from [26] and [36], the small-signal parameters of the GeSn HBT were calculated using the equivalent circuit model [37] to determine the SNR.

IV. RESULTS AND DISCUSSION

In this section, we discuss the effects of various parameters on the current gain, including those of the emitter and base layers and the Sn composition. The effect of the collector thickness was not considered in this study because its variation has negligible effect on the current gain [28], [38]. The main factors influencing the current gain are the base transmission and emitter injection efficiencies. These factors are strongly influenced by the base and emitter layer thicknesses [28], [38]. A high collector breakdown voltage can be obtained by having a low doping concentration, i.e., nearly 10^{17} cm^{-3}, in the collector, and a suggested thickness of approximately 400 nm can provide excellent device performance in terms of frequency.

A. GUMMEL PLOTS

Gummel plots provide important information about various HPT characteristics such as the recombination in the space charge region and surface recombination at the exposed layers (emitter and/or base) [39]. A Gummel plot shows the variations in the base current (I_{B}) and collector current (I_{C})

with change in the applied base-emitter voltage (V_{BE}), and their ratio ($\beta = I_C/I_B$) is defined as the current gain. Figure 2 shows the Gummel plot calculated for a fixed collector–emitter voltage (V_{CE}) of -1 V and a base–collector voltage (V_{BC}) of 0 V with $x = 6\%$ in the GeSn base layer. As V_{BE} increases, I_C continuously increases but tends to saturate starting at $V_{BE} \approx -0.5$ V. On the other hand, I_B decreases at low V_{BE} and continuously increases as V_{BE} increases further. This reversal/dip behavior of the base current at $V_{BE} \approx -0.095$ V can be explained based on the negative base current generated due to optical absorption in the base–collector region. Upon increasing the applied V_{BE} further, the electrical current dominates the photo-generated base current, generating a peak in the gain plot, as shown in Fig. 2. It is clear that the current gain is nearly constant between $V_{BE} \approx -0.1$ V and $V_{BE} \approx -0.5$ V. The gain decreases after $V_{BE} \approx -0.5$ V because the base current increases more than the collector current at higher bias voltages in this structure. Therefore, the operational range for V_{BE} was chosen to be from -0.1 V to -0.5 V to maintain a stable photocurrent output.

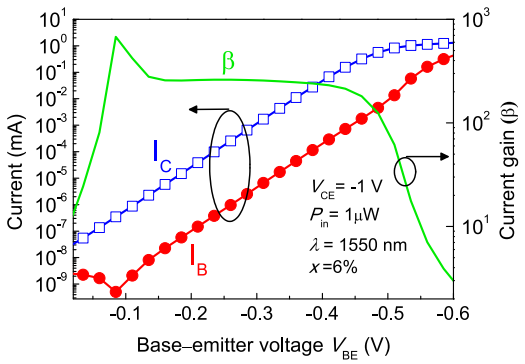

FIGURE 2. Variations of collector current, base current and current gain with applied base emitter voltage for a constant collector emitter voltage of -1 V and $x = 6\%$.

B. EFFECTS OF BASE LAYER ON CURRENT GAIN

In this section, the effects of base thickness (t_B) and doping concentration (N_B) on the current gain are described. We first discuss the effects of the base thickness on the current gain. The current gain was calculated as a function of the base thickness for different Sn compositions in the base layer with N_B fixed at 1×10^{18} cm^{-3}. The results are displayed in Fig. 3(a), which demonstrates that the current gain strongly depends on the base thickness. Specifically, it decreases with increasing base thickness. This observation can be explained by the fact that the base transmission efficiency decreases with increasing base thickness, thereby decreasing the current gain [38]. Thus, a small base layer thickness is preferred for achieving high current gain, and a reasonable base thickness of 50 nm was used in this study to optimize the base doping concentration.

Next, we examined the effects of the base doping concentration on the current gain. Assuming that all of the structural

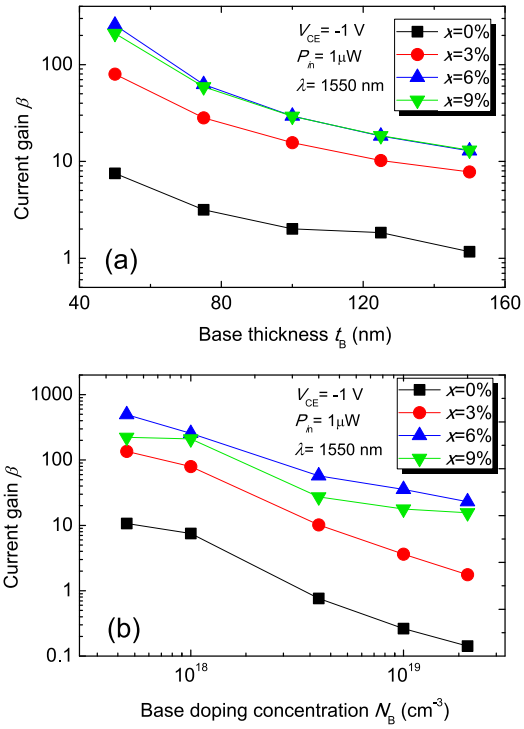

FIGURE 3. Variations in current gain (a) with change in the base thickness and (b) with change in the base doping concentration for a fixed base thickness of 50 nm. The other parameters are listed in Table 1.

parameters had the values shown in Table 1 with a fixed base thickness of 50 nm, the current gains were calculated with different base doping concentrations for different Sn compositions, and the results are presented in Fig. 3(b). The current gain clearly decreases with increasing base doping concentration. With a heavily doped base, impurity scattering reduces the hole minority diffusion length and carrier lifetime [37]. The base–collector space charge region also decreases with increasing base doping level. These results suggest that a low base doping level is preferable for achieving high current gains. However, to achieve high-frequency operation, a heavily doped base is preferred to reduce the base resistance. Thus, the base doping concentration must be optimized so that a large current gain (large diffusion length of carriers), low base resistance, and high-frequency capabilities can be simultaneously achieved. Consequently, $N_B = 1 \times 10^{18}$ cm^{-3} was considered optimal in this work.

C. EFFECTS OF EMITTER LAYER ON CURRENT GAIN

We next examined the effects of the emitter thickness (t_E) on the current gain. For a fixed emitter doping level (P_E) of 1×10^{18} cm^{-3}, Fig. 4(a) shows the current gain as a function of the emitter thickness for different Sn compositions in the base layer. With increasing emitter thickness, the current gain slightly increases for all Sn compositions due to the small increase in the photocurrent contribution of the collector region. However, the contribution of this photocurrent is not significant when compared with the photocurrent generated

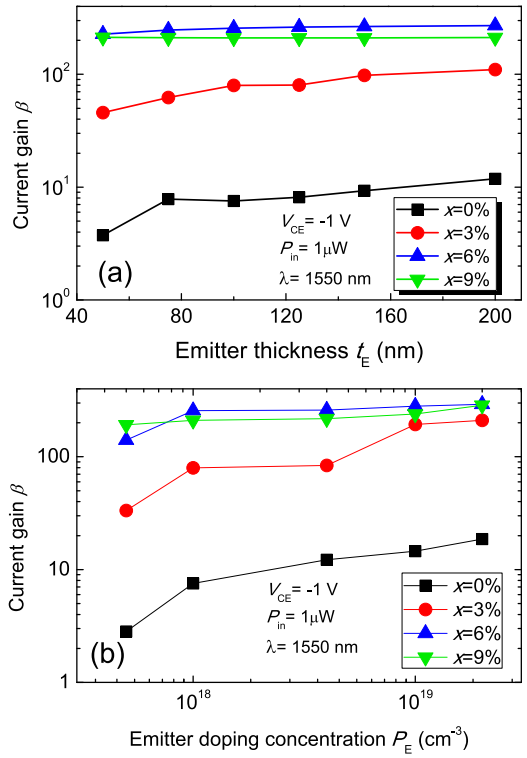

FIGURE 4. **Variations in current (a) with change in the emitter thickness and (b) with change in the emitter doping concentration for a fixed emitter thickness of 100 nm and different Sn compositions.**

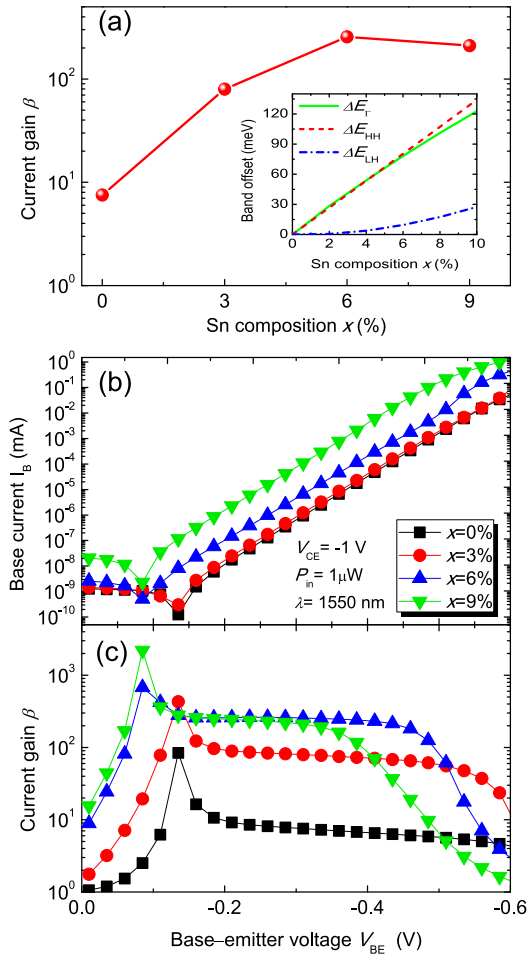

FIGURE 5. **(a) Current gain variation with Sn composition in the $Ge_{1-x}Sn_x$ base with optimized layer parameters. The inset shows the valence band offsets between the Ge and pseudomorphic $Ge_{1-x}Sn_x$ on Ge as a function of Sn composition. (b) Variation in base currant and (c) variation in current gain with change in applied base emitter voltage for different Sn concentrations in the $Ge_{1-x}Sn_x$ base.**

in the absorption region. Therefore, the current gain is less dependent on the emitter thickness, and $t_E = 100$ nm was chosen for optimizing the HPT structures.

Figure 4(b) shows the variation in the current gain with change in the emitter doping concentration with a fixed t_E of 100 nm and different Sn concentrations, demonstrating that the current gain increases with increasing emitter doping concentration. Therefore, a high emitter doping concentration is desired to enhance the current gain. The injection efficiency in a bipolar junction transistor can be increased by increasing the ratio between the emitter and base doping concentrations, thereby enhancing the current gain. A high emitter doping concentration in an HPT could lead to a significant increase in the current gain. However, a heavily doped emitter will cause a capacitive effect and high tunneling current at the junction, leading to degradation of the frequency and direct current performance [39]. Hence, the emitter doping optimization is very important to balance these effects as well as to maintain a high current gain. Thus, $P_E = 1 \times 10^{18}$ cm^{-3} was determined to be optimal in this work.

D. EFFECTS OF SN COMPOSITION ON CURRENT GAIN

The current gains of HPTs with different Sn concentrations in the $Ge_{1-x}Sn_x$ base were calculated based on the above-mentioned optimized layer parameters, t, and the results are depicted in Fig. 5(a). The current gain increases with increasing Sn composition (up to $x = 6\%$) for the proposed device structure. As the Sn concentration increases further, the current gain gradually decreases. The increase in current gain can be explained based on the increased bandgap difference (ΔE_g) between the $Ge_{1-x}Sn_x$ base and the Ge emitter region, as shown in the inset of Fig. 5(a). The Ge emitter region has a larger bandgap than the $Ge_{1-x}Sn_x$ base region. This bandgap difference prevents the backward injection of electrons from the base region due to the large hetero-barrier at the valance band. Consequently, carriers can be accumulated in the base region to lower the emitter–base barrier, allowing the injection of holes from the emitter region into the base region to enhance the current gain. These results suggest that there is an optimal Sn composition for the proposed $Ge_{1-x}Sn_x$ *p-n-p* HPTs that will maximize the current gain. The collector current increases upon increasing the Sn concentration from 0% to 9% in the GeSn base. However, the base current also increases with increasing Sn concentration,

as shown in Fig. 5(b). The base current increase in the case of 9% Sn is the cause of the lower current gain. Figure 5(c) shows the variation in the current gain with change in the applied base-emitter voltage. Increasing the Sn concentration evidently shifts the maximum gain point toward less negative V_{BE} values because of the reduced bandgap of the GeSn base. Therefore, the V_{BE} required for stable current gain output is reduced, which is beneficial for reducing the power consumption of the device.

E. SIGNAL-TO-NOISE RATIO

Another advantage of using HPTs in optical communication networks is the appreciable SNR for high-speed operation. Figure 6 shows the calculated SNR as a function of the operating frequency at the HPT output for different Sn concentrations in the base layer with an input resistance (R_i) of 10 kΩ and an incident optical power of 1 μW at 1550 nm wavelength. The calculation results show that the SNR decreases rapidly with increasing HPT operating frequency beyond 1 GHz due to the precipitous increase in the mean square shot noise current component at the base–collector junction. This current is strongly affected by the randomness of photon arrival and excess carrier generation in the junction and it eventually causes the SNR to decrease beyond 1 GHz. The SNR increases as the Sn content increases from 0% (pure Ge) to 3%. This behavior is attributed to the voltage gain, which increases as the Sn content increases from 0% (pure Ge) to 3%, thereby increasing the output signal power. The increase in signal power leads to an increase in the SNR. As the Sn content increases further, the SNR decreases because the mean square shot noise power increases steeply at the B-E and B-C junctions for the Sn concentrations of 6% and 9%. Nevertheless, the SNRs calculated for the GeSn HPTs can exceed 20 dB in the operating frequency range up to 100 GHz, and meet the typical requirements of >20 dB for practical applications. Therefore, these results suggest that the GeSn HPTs can achieve high-speed, low-noise optical detection.

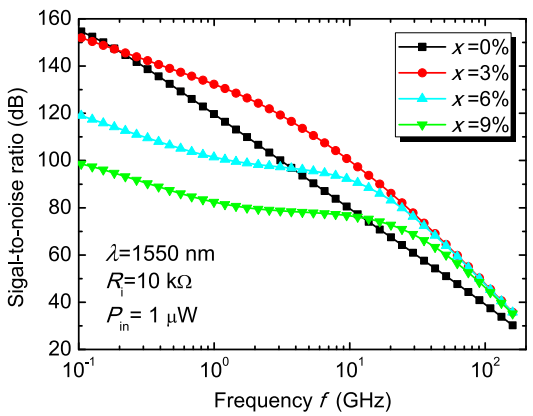

FIGURE 6. Calculated SNR as a function of applied frequency for different Sn compositions in the $Ge_{1-x}Sn_x$ base.

F. EFFECTS OF SiO_2 ANTI-REFLECTION LAYER ON HPT REFLECTIVITY

Generally, to improve the light gathering capacity of a device, the exposed layers are covered with SiO_2 AR coating, which enhances the photocurrent generation due to the reduced reflection of the incident light. To optimize the thickness of the SiO_2 AR layer (t_{OX}), the reflectivity of the HPT device was calculated as a function of the SiO_2 AR layer using the transfer matrix method, where the wavelength-dependent refractive indices of the materials were obtained from [36], [40], and [41]. The calculated reflectivity spectra in the wavelength range from 1.2 μm to 2.2 μm for $x = 9\%$ are displayed in Fig. 7. As shown, there are ripples in the reflectivity spectra because of the interference between the layers. The reflectivity is between 0.35 and 0.45 when there is no SiO_2 AR coating. Increasing the thickness of the SiO_2 coating can significantly decrease the reflectivity, permitting more photons to enter the HPTs and thus enhancing the responsivity. When the thickness is increased beyond 300 nm, the reflectivity increases at lower wavelengths whereas it slightly decreases at longer wavelengths. Therefore, the optimal SiO_2 thickness is between 200 nm and 300 nm, and $t_{OX} = 300$ nm was adopted for the responsivity calculations in this study (the same results were obtained for different Sn contents in the $Ge_{1-x}Sn_x$ base layer).

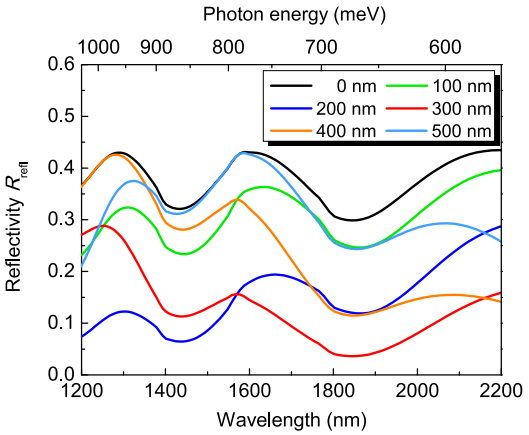

FIGURE 7. Simulated reflectivity variations with wavelength for a $Ge_{0.91}Sn_{0.09}$ HPT for different AR SiO_2 thicknesses.

G. OPTICAL ABSORPTION AND RESPONSIVITY

After determining the optimal current gain, we finally calculate the optical responsivity spectra of the proposed *p-n-p* $Ge_{1-x}Sn_x$ HPTs. The calculated absorption coefficient spectra for pseudomorphic $Ge_{1-x}Sn_x$ on Ge are displayed in Fig. 8(a), and the calculated optical responsivity spectra for the *p-n-p* $Ge_{1-x}Sn_x$ HPTs are depicted in Fig. 8(b). Figure 8(a) demonstrates that the absorption spectrum is extended to longer wavelengths with increasing Sn content, because of the direct bandgap shrinkage caused by Sn alloying. Consequently, the absorption range and efficiency in the infrared range can be improved by introducing Sn into the

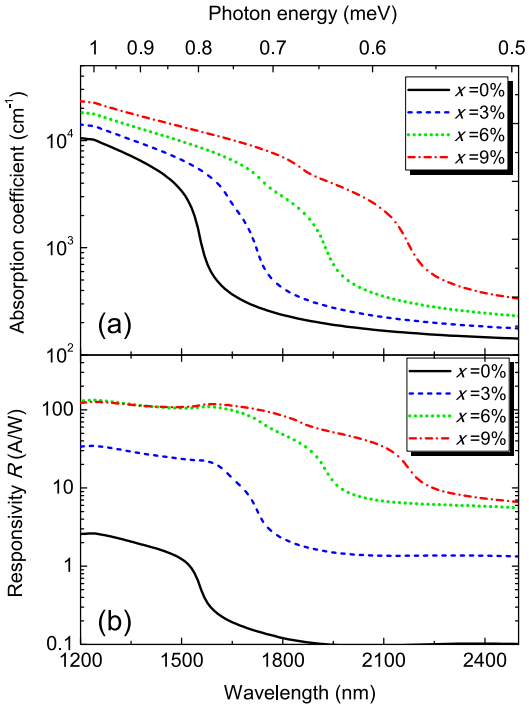

FIGURE 8. **(a) Calculated absorption coefficient spectra for pseudomorphic $Ge_{1-x}Sn_x$ on Ge. (b) Calculated optical responsivity spectra for the *p-n-p* $Ge_{1-x}Sn_x$ HPTs.**

$Ge_{1-x}Sn_x$ base layer. The responsivity for the $x = 0\%$ case (pure Ge) gradually decreases with increasing wavelength and then reaches a cutoff point at 1550 nm, corresponding to the direct bandgap energy (0.8 eV). As the Sn content increases, the photodetection cutoff point is shifted to 1920 nm for $x = 6\%$ and 2220 nm for $x = 9\%$ because of the direct bandgap shrinkage caused by Sn alloying. In addition, the responsivity considerably increases to tens of amps per watt. This behavior is attributed to the enhanced current gain, which is much higher than it is in GeSn based PDs (<1 A/W) [22]. These results suggest that optimized *p-n-p* GeSn HPTs can achieve high-performance photodetection in the infrared region.

H. EFFECTS OF INTERFACES AND DEFECTS ON CURRENT GAIN

In HTPs, interfaces and defect density may influence the current gain [42]. In the $Ge_{1-x}Sn_x$ HPTs, increasing the Sn composition leads to larger lattice mismatch between GeSn and Ge VS, which may increase the misfit dislocations at the heterointerfaces. As a result, the minority carrier lifetime (τ_p) and diffusion length (L_p) may decrease because of increased defect density and degraded heterointerfaces, thereby reducing the current gain. (We have considered L_p here because the GeSn base region is *n*-doped, because of which holes will be the minority carries. The relationship between the minority carrier lifetime and the diffusion length is $L_p = \sqrt{\tau_p D_p}$, where D_p is the hole diffusion constant. Here $D_p = 49 \times 10^{-4}$ m^2/s [26] is used in the calculations.) To

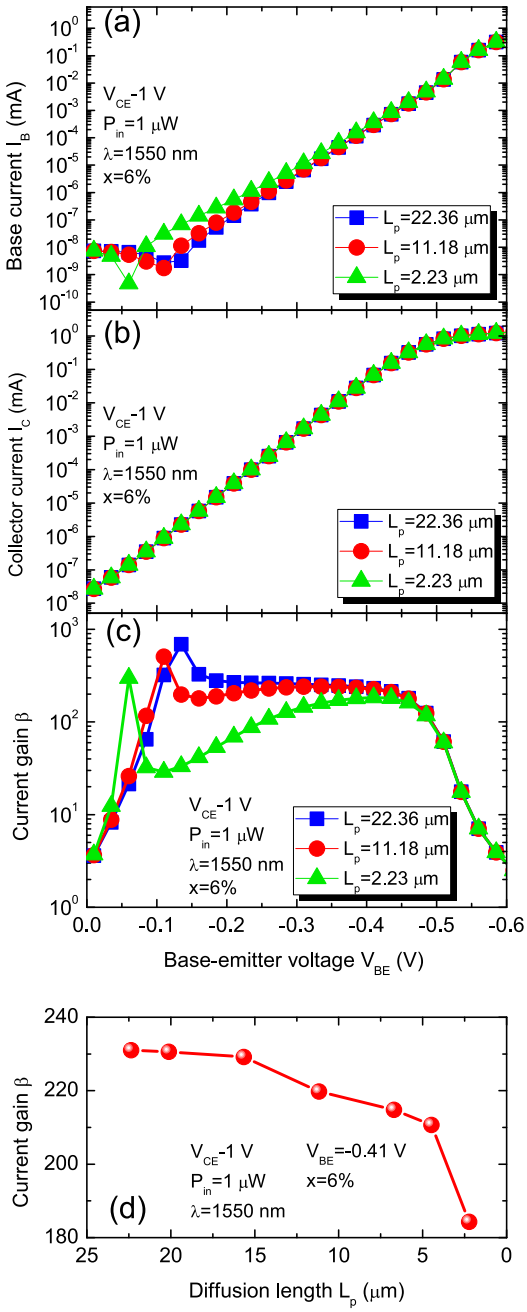

FIGURE 9. **(a) Calculated base current, (b) collector current, (c) current gain as a function of the base-emitter voltage for different minority carrier diffusion lengths. (d) Calculated current gain as a function of minority carrier diffusion length.**

study the impact of the heterointerfaces and defects on current gain, we calculate the current gain for the GeSn HPTs ($x = 6\%$) with different diffusion lengths. The Gummel plots and the calculated current gain are depicted in Fig. 9. As L_p decreases, the base current increases as shown in Fig. 9(a) because of higher electron-hole recombination rate in the base region. On the other hand, the collector current does not have a significant dependence on L_p as shown

in Fig. 9(b). Therefore, the current gain decreases upon decreasing L_p, as shown in Fig. 9(c). Figure 9(d) shows the calculated current gain as a function of L_p. As L_p decreases, the current gain decreases from 231.0 for $L_p = 22.6$ μm to 184.3 for $L_p = 2.26$ μm, suggesting a 20.3% decrease. Considering that the achievable gain still remains high for the optimized GeSn HPTs, the reduction in current gain due to defects and misfit dislocations at the heterointerfaces is actually not significant. These results suggest that high current gain is still achievable in the optimized GeSn HPTs even in the presence of defects and misfit dislocations at the heterointerfaces. In addition, the entire HPT structure can be grown on a strain-relaxed SiGeSn VS, and the Ge collector and emitter can be potentially replaced with lattice matched SiGeSn layers which allow for independently turning the bandgap energy and lattice constant. As a result, a strain-free *p-n-p* SiGeSn/GeSn/SiGeSn based HPT is possible to significantly reduce the interface and defect states in the device. By carefully designing and optimizing the SiGeSn collector and emitter, the performance of the device may be further enhanced. Such *p-n-p* SiGeSn/GeSn/SiGeSn based HPTs can be explored as future aspect of high-performance Si-based infrared HPTs for a wide range of applications.

V. CONCLUSION

We presented the design and a comprehensive study of *p-n-p* GeSn HPTs. The analysis results show that the current gain strongly depends on the base thickness, base doping concentration, emitter doping concentration, and Sn concentration in the GeSn base. Optimizing the structural parameters can significantly enhance the current gain, thereby enhancing the quantum efficiency. In addition, increasing the Sn content in the base can considerably reduce the bandgap energy, thus extending the photodetection range in the infrared. The SNR analysis revealed a strong dependence on the operation frequency and Sn composition in the base of the GeSn HPTs, and a good SNR of >20 dB is achievable. With CMOS compatibility, high current gains, wide photodetection ranges in the infrared region, and good SNRs at high operation frequencies, the proposed *p-n-p* GeSn HPTs are expected to be capable of high-performance photodetection for a wide range of important applications.

ACKNOWLEDGMENT

The authors thank Prof. Henry H. Cheng at National Taiwan University, Taipei, Taiwan for many insightful discussions. A. K. Pandey and H. Kumar would like to thank AIM-HI, National Chung Cheng University, Taiwan for providing the research opportunity.

REFERENCES

[1] M. N. Abedin, T. F. Refaat, O. V. Sulima, and U. N. Singh, "AlGaAsSb-InGaAsSb HPTs with high optical gain and wide dynamic range," *IEEE Trans. Electron Devices*, vol. 51, no. 12, pp. 2013–2018, Dec. 2004.

[2] R. Basu, V. Chakraborty, B. Mukhopadhyay, and P. K. Basu, "Signal-to-noise ratio for a Ge-GeSn-GeSn hetero phototransistors at 1.55 μm," in *Proc. 6th Int. Conf. Comput. Devices Commun. (CODEC)*, 2015, pp. 16–19.

[3] M. J. Deen and P. K. Basu, *Silicon Photonics: Fundamentals and Devices*. Chichester, U.K.: Wiley, 2012.

[4] K.-W. Ang, M.-B. Yu, G.-Q. Lo, and D.-L. Kwong, "Low-voltage and high-responsivity germanium bipolar phototransistor for optical detections in the near-infrared regime," *IEEE Electron Device Lett.*, vol. 29, no. 10, pp. 1124–1127, Oct. 2008.

[5] S.-W. Tan *et al.*, "Characterization and modeling of three-terminal heterojunction phototransistors using an InGaP layer for passivation," *IEEE Trans. Electron Devices*, vol. 52, no. 2, pp. 204–210, Feb. 2005.

[6] M. S. Park and J. H. Jang, "Enhancement of optical gain in floating-base InGaP-GaAs heterojunction phototransistors," *IEEE Photon. Technol. Lett.*, vol. 22, no. 16, pp. 1202–1204, Aug. 15, 2010.

[7] H. A. Khan, A. A. Rezazadeh, and S. Sohaib, "Modeling and analysis of the spectral response for AlGaAs/GaAs HPTs for short wavelength optical communication," *J. Appl. Phys.*, vol. 109, no. 10, 2011, Art. no. 104507.

[8] A. Dehzangi, A. Haddadi, S. Adhikary, and M. Razeghi, "Impact of scaling base thickness on the performance of heterojunction phototransistors," *Nanotechnology*, vol. 28, no. 10, 2017, Art. no. 10LT01.

[9] K. Xu *et al.*, "Light emitting devices in Si CMOS and RF bipolar integrated circuits," *J. Illum. Eng. Soc.*, vol. 12, no. 4, pp. 203–212, 2016.

[10] X. W. Wang *et al.*, "Enhanced thermoelectric figure of merit in nanostructured *n*-type silicon germanium bulk alloy," *Appl. Phys. Lett.*, vol. 93, no. 19, 2008, Art. no. 193121.

[11] W.-K. Chen, *VLSI Technology*. Boca Raton, FL, USA: CRC Press, 2007.

[12] K. Xu, "Monolithically integrated Si gate-controlled light-emitting device: Science and properties," *J. Opt.*, vol. 20, no. 2, 2018, Art. no. 024014.

[13] S. Villa, A. L. Lacaita, L. M. Perron, and R. Bez, "A physically-based model of the effective mobility in heavily-doped n-MOSFETs," *IEEE Trans. Electron Dev.*, vol. 45, no. 1, pp. 110–115, Jan. 1998.

[14] K. Xu, "Integrated silicon directly modulated light source using p-well in standard CMOS technology," *IEEE Sensors J.*, vol. 16, no. 16, pp. 6184–6191, Aug. 2016.

[15] E. Kasper, M. Kittler, M. Oehme, and T. Arguirov, "Germanium tin: Silicon photonics toward the mid-infrared [invited]," *Photon. Res.*, vol. 1, no. 2, pp. 69–76, 2013.

[16] R. Roucka *et al.*, "High-performance near-IR photodiodes: A novel chemistry-based approach to Ge and Ge–Sn devices integrated on silicon," *IEEE J. Quantum Electron.*, vol. 47, no. 2, pp. 213–222, Feb. 2011.

[17] S. Su *et al.*, "GeSn p-i-n photodetector for all telecommunication bands detection," *Opt. Exp.*, vol. 19, no. 7, pp. 6400–6405, 2011.

[18] M. Oehme *et al.*, "GeSn p-i-n detectors integrated on Si with up to 4% Sn," *Appl. Phys. Lett.*, vol. 101, no. 14, 2012, Art. no. 141110.

[19] H. H. Tseng *et al.*, "GeSn-based p-i-n photodiodes with strained active layer on a Si wafer," *Appl. Phys. Lett.*, vol. 103, no. 23, 2013, Art. no. 231907.

[20] Y. H. Peng, H. H. Cheng, V. Mashanov, and G.-E. Chang, "GeSn p-i-n waveguide photodetectors on silicon substrates," *Appl. Phys. Lett*, vol. 105, no. 23, 2014, Art. no. 231109.

[21] T. Pham *et al.*, "Systematic study of Si-based GeSn photodiodes with 2.6 μm detector cutoff for short-wave infrared detection," *Opt. Exp.*, vol. 24, no. 5, pp. 4519–4531, 2016.

[22] B.-J. Huang, J.-H. Lin, H. H. Cheng, and G. E. Chang, "GeSn resonant-cavity-enhanced photodetectors on silicon-on-insulator platforms," *Opt. Lett.*, vol. 43, no. 6, pp. 1215–1218, 2018.

[23] V. R. D'Costa *et al.*, "Sn-alloying as a means of increasing the optical absorption of Ge at the C- and L-telecommunication bands," *Semicond. Sci. Technol.*, vol. 24, no. 11, 2009, Art. no. 115006.

[24] M. Oehme *et al.*, "Epitaxial growth of strained and unstrained GeSn alloys up to 25% Sn," *Thin Solid Films*, vol. 557, pp. 169–172, Apr. 2014.

[25] G.-E. Chang, R. Basu, B. Mukhopadhyay, and P. K. Basu, "Design and modeling of GeSn-based heterojunction phototransistors for communication applications," *IEEE J. Sel. Topics Quantum Electron.*, vol. 22, no. 6, Nov./Dec. 2016, Art. no. 8200409.

[26] R. Basu, V. Chakraborty, B. Mukhopadhyay, and P. K. Basu, "Predicted performance of Ge/GeSn hetero-phototransistors on Si substrate at 1.55 μm," *Opt. Quantum Electron.*, vol. 47, no. 2, pp. 387–399, 2014.
[27] D. V. Kumar, A. K. Pandey, R. Basu, and A. K. Sharma, "Simulated characteristics of a heterojunction phototransistor with $Ge_{1-x}Sn_x$ alloy as base," *Opt. Eng.*, vol. 55, no. 12, 2016, Art. no. 127103.
[28] A. K. Pandey, R. Basu, and G.-E. Chang, "Optimized $Ge_{1-x}Sn_x$ multiple-quantum-well heterojunction phototransistors for high-performance SWIR photodetection," *IEEE Sens. J.*, vol. 18, no. 14, pp. 5842–5852, Jul. 2018.
[29] W. Wang *et al.*, "Floating-base germanium-tin heterojunction phototransistor for high-efficiency photodetection in short-wave infrared range," *Opt. Exp.*, vol. 25, no. 16, pp. 10170–10173, 2017.
[30] H. Shao, W. Li, A. Torfi, D. Moscicka, and W. I. Wang, "Room-temperature p-n-p AlGaAsSb-InGaAsSb heterojunction phototransistors with cutoff wavelength at 2.5 μm," *IEEE Photon. Technol. Lett.*, vol. 18, no. 22, pp. 2326–2328, Nov. 15, 2006.
[31] S. Frimel, K. Roenker, B. H. K. Gummel, and H. C. Poon, "Gummel–Poon model for NPN heterojunction bipolar phototransistors," *J. Appl. Phys.*, vol. 82, no. 7, pp. 3581–3592, 1997.
[32] T. Conklin *et al.*, "Inclusion of tunneling and ballistic transport effects in an analytical approach to modeling of NPN InP-based heterojunction bipolar transistors," *Superlattices Microstruct.*, vol. 18, no. 1, pp. 21–32, 1995.
[33] M. Oehme, J. Werner, and E. Kasper, "Molecular beam epitaxy of highly antimony doped germanium on silicon," *J. Cryst. Growth*, vol. 310, no. 21, pp. 4531–4534, 2008.
[34] S. V. Golod, V. Y. Prinz, V. I. Mashanov, and A. K. Gutakovsky, "Fabrication of conducting GeSi/Si micro- and nanotubes and helical microcoils," *Semicond. Sci. Technol.*, vol. 16, no. 3, pp. 181–185, 2001.
[35] W. Wang, Q. Zhou, Y. Dong, E. S. Tok, and Y.-C. Yeo, "Critical thickness for strain relaxation of $Ge_{1-x}Sn_x$ ($x \leq 0.17$) grown by molecular beam epitaxy on Ge(001)," *Appl. Phys. Lett.*, vol. 106, no. 23, 2015, Art. no. 232106.
[36] G. E. Chang, S. W. Chang, and S. L. Chuang, "Strain-balanced Ge_zSn_{1-z}–$Si_xGe_ySn_{1-x-y}$ multiple-quantum-well lasers," *IEEE J. Quantum Electron.*, vol. 46, no. 12, pp. 1813–1820, Dec. 2010.
[37] P. Chakrabarti, N. K. Agrawal, P. Kalra, S. Agrawal, and G. Gupta, "Noise modeling of an InP/InGaAs heterojunction bipolar phototransistor," *Opt. Eng.*, vol. 42, no. 4, pp. 939–947, 2003.
[38] Y. Zhang, C. Li, S.-Y. Chen, H.-K. Lai, and J.-Y. Kang, "Numerical analysis of SiGe heterojunction bipolar phototransistor based on virtual substrate," *Solid-State Electron.*, vol. 52, no. 11, pp. 1782–1790, 2008.
[39] R. Sridhara, S. M. Frimel, K. P. Roenker, N. Pan, and J. Elliott, "Performance enhancement of GaInP/GaAs heterojunction bipolar phototransistors using DC base bias," *J. Lightw. Technol.*, vol. 16, no. 6, pp. 1101–1106, 1998.
[40] E. D. Palik, *Handbook of Optical Constants of Solids*. Orlando, FL, USA: Academic, 1985.
[41] R. E. Lindquist and A. W. Ewald, "Optical constants of single-crystal gray tin in the infrared," *Phys. Rev.*, vol. 35, no. 1A, pp. 191–194, 1964.
[42] H. T. Lin, D. H. Rich, O. Sjolund, M. Ghisoni, and A. Larsson, "Influence of structural defects on carrier recombination and current gain in an InGaAs/AlGaAs/GaAs heterojunction phototransistor," *J. Appl. Phys.*, vol. 79, no. 10, pp. 8015–8023, 1996.

ANKIT KUMAR PANDEY (S'16) received the B.Tech. degree from the United College of Engineering and Research, Allahabad, India, in 2012, the M.Tech. degree from the J.K. Institute of Applied Physics and Technology, University of Allahabad, India, in 2014, and the Ph.D. degree from the ECE Department, National Institute of Technology Delhi, India, where he is currently a Research Associate with the Department of Applied Sciences. His research areas are optical photodetectors and SPR-based sensors.

RIKMANTRA BASU (M'15) received the B.Sc., B.Tech., M.Tech., and Ph.D. degrees from the University of Calcutta in 2004, 2007, 2009, and 2013, respectively, where he joined as an SRF with the Center for Research in Nanoscience and Nanotechnology in 2009 and continued as a CSIR SRF. He served as an Assistant Professor with the Birla Institute of Technology and Science, Pilani, from 2013 to 2014. Since 2014, he has been an Assistant Professor with the ECE Department, National Institute of Technology Delhi. He was with the University of Bristol in 2014 and has engaged in research with the National Chun Cheng University, Taiwan, as a Visiting Researcher in 2017. He has also visited Canada, USA, South Korea, Denmark, Singapore, and many other countries to present his research. He has authored numerous journals and conference publications, contributed two chapters in edited volumes, and co-authored a book entitled *Semiconductor Laser Theory* (CRC Taylor and Francis, 2015). His research areas are transistor lasers, group IV photonics, and VLSI design. He was a recipient of the Young Scientist Award at the URSI General Assembly in 2012, held in Istanbul, Turkey. He has served as the President of IEEE Student Branch of CU. He is a member of APS and OSA.

HARSHVARDHAN KUMAR received the Bachelor of Engineering degree from Nagpur University, India, in 2014, the Master of Engineering degree from Amravati University, India, and the M.Tech. degree from Central Scientific Instruments Organization, Chandigarh, India, in 2017. He is currently pursuing the Ph.D. degree with the ECE Department, National Institute of Technology Delhi. His research areas are semiconductor and photonic devices.

GUO-EN CHANG (S'09–M'10) received the B.S. degree from the Department of Mechanical Engineering, National Cheng Kung University, Tainan, Taiwan, in 2003 and the Ph.D. degree from the Institute of Applied Mechanics, National Taiwan University, Taipei, Taiwan, in 2010.

He was a Visiting Scholar with the University of Illinois at Urbana–Champaign, Urbana, from 2007 to 2009, and a Post-Doctoral Fellow with National Taiwan University from 2010 to 2011. In 2011, he joined the Department of Mechanical Engineering, National Chung Cheng University, Chiayi, Taiwan, where he is currently an Associate Professor. He received the Graduate Student Study Abroad Program Award from the National Science Council of Taiwan to visit the University of Illinois at Urbana–Champaign from 2007 to 2009. His current research interests include silicon photonics, bio-photonics, sensors and actuators, and precision optical measurements. He was a recipient of the Excellent Young Innovator Award from the Taiwan Comprehensive University System in 2014 and 2015, the Young Scholar Award from the College of Engineering, National Chung Cheng University in 2014, the Outstanding Mechanical Engineer Award, the Outstanding Young Mechanical Faculty Award in 2015, and the Outstanding Mechanical Professor Award in 2018 from the Chinese Society of Mechanical Engineers. He is a Senior Member of the Optical Society of America, and a member of the International Society for Optics and Photonics and the Chinese Society of Mechanical Engineers.